Gallium-related 0.875-eV photoluminescence defect spectrum in irradiated silicon

K. Thonke, N. Bürger, and R. Sauer
Physikalisches Institut (Teil 4), Universität Stuttgart, D-7000 Stuttgart 80 (Vaihingen), Pfaffenwaldring 57, Federal Republic of Germany
(Received 21 December 1984; revised manuscript received 14 May 1985)

The 0.875-eV (Ga1) photoluminescence defect spectrum in gallium-doped irradiated silicon is studied in high resolution and in uniaxial stress and homogeneous magnetic fields. The spectrum exhibits one- and two-phonon Stokes satellites of the no-phonon Ga1 line due to the coupling of quasilocalized vibrational modes of quantum energy $\hbar\omega = 56.3$ meV. Temperature-controlled measurements reveal two electronic excited states at energies of 5.1 and 6.0 meV in excess of the upper Ga1 level. These three states are strongly mixed by uniaxial stress resulting in a nonlinear stress response. The symmetry of the defect is determined to be rhombic I (C_{2v}) from the linear portion of the stress response. Complicated Zeeman spectra of Ga1 are fully identified as spin-$\frac{1}{2}$—to—spin-$\frac{1}{2}$ transitions at a center of C_{2v} point-group symmetry. An isotope effect observed in ^{13}C-enriched silicon gives evidence that the optical defect incorporates carbon in addition to gallium. A defect model is discussed on the basis of the experimental results.

I. INTRODUCTION

In 1974, Noonan *et al.*[1] reported three photoluminescence (PL) lines at energies of 0.875 eV (Ga1), 1.049 eV (Ga2), and 0.926 eV (Ga3). They appeared exclusively in Ga-doped silicon in distinct annealing stages after electron irradiation at doses around 10^{17} cm^{-2} and at a temperature of -10 °C. That previous work[1] mainly aimed at an investigation of the Ga and Al doping effects on other PL lines which likewise originate in irradiation induced defects [viz., the G line at 0.97 eV (Refs. 2—4) and the C line at 0.79 eV (Refs. 5—7)]; therefore, only survey spectra at a small resolution ($\delta E \gtrsim 2$ meV) were recorded, and particular emphasis was laid on a comparison of the annealing behavior of the various PL lines. The line of interest here, Ga1, grew in above 100 °C, peaked at 200 °C, and was entirely quenched at 250 °C. (The annealing data of Noonan *et al.*[1] are redrawn in Fig. 1.) It was found that Ga doping degraded the intensity of the G line which is known to be emitted by an optical center incorporating two substitutional carbon atoms and a silicon interstitial.[3,4]

Recent work on the Ga-related spectra concerns Ga2 and Ga1. Elliott[8] reported that the Ga2 spectrum shows singlet and triplet no-phonon lines with an anisotropic Zeeman splitting of the triplet which he could not explain in detail. The Ga1 spectrum was studied by Thonke *et al.*,[9] who found that carbon is incorporated as well in the optical defect, and determined the symmetry of the defect to be rhombic I (C_{2v}) without communicating the piezo-optic constants. The same symmetry classification was arrived at by Clifton *et al.*[10] in their stress study of the Ga1 spectrum.

The present paper is a comprehensive report on our study of the Ga1 spectrum. Among the new results obtained is the observation of two electronic excited states explaining the nonlinear dependence of the Ga1 line on stress. A full explanation of the complicated Zeeman spectra is also given in terms of a spin-$\frac{1}{2}$—to—spin-$\frac{1}{2}$ transition with g values indicating that the rhombic defect strongly binds a hole whose orbital momentum is quenched and which captures an electron bound in an isotropic shallow state. The Ga1 center is the first example of a rhombic luminescent defect in silicon and clearly exhibits details of rhombic anisotropy in the stress and Zeeman spectra. This motivates us to derive the corresponding interaction matrices in two appendixes for the discussion of our data.

Standard experimental equipment was used. The photoluminescence was excited by a Kr-ion laser (647 nm, ≤ 500 mW) and dispersed by a monochromator of 1 m focal length (Spex Industries 1702) equipped with a grating of 600 grooves/mm. The signals were detected by a cooled Ge detector (North Coast) with metal shielding and electronic spike suppression, and were processed by conventional lock-in technique. In most of the experiments the samples were immersed in liquid helium; how-

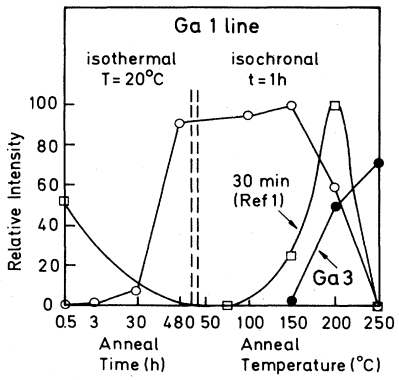

FIG. 1. Isothermal and isochronal anneal data on the Ga1 (0.875 eV) line (open circles). Solid circles refer to the Ga3 (0.929 eV) line. Open squares are data from Noonan *et al.* (Ref. 1).

ever, an evaporation cryostat with gaseous helium as the coolant was also employed. In this operation mode high optical powers (up to 100 mW) could be used at defined temperatures enabling the detection of the very weak excited states. The magnetic fields ($B \leq 5.3$ T) in the Zeeman measurements were generated by a cryomagnet in a split-coil configuration allowing light detection with the wave vector **k** perpendicular (Voigt configuration) and parallel (Faraday configuration) to the magnetic field **B**.

This paper is organized in six sections, presenting basic spectra, annealing data, and temperature-controlled photoluminescence (Sec. II), isotope effects (Sec. III), uniaxial stress measurements (Sec. IV), Zeeman data (Sec. V), and a discussion of the results (Sec. VI).

II. APPEARANCE AND FORM OF THE Ga1 SPECTRUM

In our experiments the Ga1 spectrum was generated by electron irradiation (1.5 MeV, 10^{17} e/cm^2 at low temperatures, $T \approx 100$ K) of floating-zone or pulled Ga-doped silicon. The Ga concentrations ranged from $\leq 8\times10^{14}$ to 2×10^{18} cm^{-3}. An exception is the ^{13}C-enriched sample, where ^{69}Ga was implanted. The spectrum is found to grow in only after a few days of room-temperature storage (Fig. 1). Upon subsequent isochronal annealing for 1 h, the intensity is virtually constant up to an annealing temperature of 150 °C, where it begins to decrease and eventually disappear at 250 °C. Noonan *et al.*[1] found a similar quenching temperature although their annealing curve at lower temperatures is rather different. Substantially lower quenching temperatures of the Ga1 line were obtained by Clifton *et al.*[10] in silicon samples doped to 5×10^{16} cm^{-3} with Ga and irradiated at room temperature with 5×10^{16} e/cm^{-2}. However, their general anneal curve is quite similar to our curve. In accordance with Fig. 1 and recently published work,[9] they also find that when Ga1 is destroyed the Ga3 spectrum comes up, possibly indicating that the Ga3 defect forms upon a modification of the Ga1 center. Furthermore, we have found that the Ga1 spectrum is degraded by higher oxygen concentrations.

The Ga1 spectrum (Fig. 2) is dominated by the narrow ($\delta E = 0.08$ meV) no-phonon (NP) transition $(Ga1)^0$ at 0.8754 eV. As is familiar from several other deep optical defects, the NP line is accompanied by broad vibronic bands (labels TA or 2TA) due to coupling to transverse-acoustic lattice phonons near the X point of the Brillouin zone. The broader underlying background extending to wavelengths as long as 1.7 μm stems from multiple coupling of the electronic $(Ga1)^0$ transition to low-energy continuum modes. Characteristic in the low-energy portion of the spectrum are the sharp resonances labeled $(Ga1)^1$ 56.3 meV below the NP line, and $(Ga1)^2$ 56.3 + 55.6 meV below the NP line. These satellites are electronic-vibronic transitions involving one or two quasi-localized modes of the defect ground state of quantum energy $\hbar\omega = 56.3$ meV in a slightly anharmonic potential. The assignment is based on the observation of the two-phonon transition $(Ga1)^2$, and on the fact that $(Ga1)^1$ splits like $(Ga1)^0$ under uniaxial stress (see Sec. IV). The linewidths at 4.2 K, $(Ga1)^0$: $\delta E = 0.08$ meV, $(Ga1)^1$: $\delta E = 1.1$ meV, are also consistent with this interpretation. The total phonon coupling to $(Ga1)^0$ is weak (Huang-Rhys factor $S_{tot} \approx 1.2$) and does not vary in the temperature range from 2 to 30 K. The electronic-vibronic transition $(Ga1)^1$ in turn couples to lattice modes producing the broad sidebands $Ta(Ga1)^1$ and $2TA(Ga1)^1$. Further lines in Fig. 2 stem from optical lattice phonons (the sharp 0^Γ peak) coupled to the $(Ga1)^0$ transition or are independent features (line C at 0.79 eV emitted by an optical defect incorporating carbon and oxygen[6,7,9]).

When the temperature is raised above 10 K we observe two extra lines coming up at higher energies than $(Ga1)^0$ displaced by $+5.1$ meV $(Ga1)^0_1$ or $+6.0$ meV $(Ga1)^0_2$ (Fig. 3). The first line has a substantially larger linewidth (0.18 meV) without detectable substructure than the latter line (0.1 meV). The change of their relative intensities in Fig. 3 from $T = 10$ to 19 K is consistent with a Boltzmann-population factor of their initial states with thermal activation energies identical to their spectroscopic

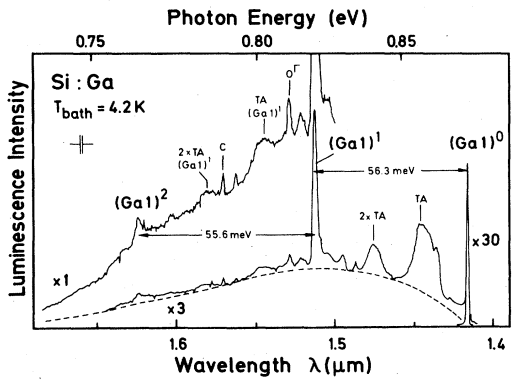

FIG. 2. Ga1 photoluminescence spectrum. Upper indices denote number of local modes coupled to the electronic transition $(Ga1)^0$; other symbols are explained in the text.

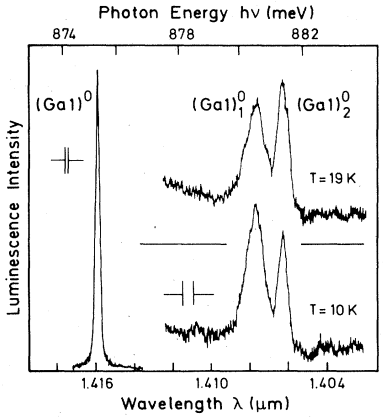

FIG. 3. Ga1 spectrum in the no-phonon region at elevated temperatures showing lines $(Ga1)^0_1$ and $(Ga1)^0_2$ originating from excited defect states. Subscripts denote numbering of electronic states.

spacing. Temperature-controlled experiments from 10 to 30 K (Fig. 4) make sure that $(Ga1)_1^0$ and $(Ga1)_2^0$ are transitions from excited defect states to the same ground state. In the measurements shown in Fig. 4 the two lines were not resolved and appear as one line which is labeled (Ga1)*. The intensity ratio of (Ga1)* to $(Ga1)^0$ follows an exponential law versus reciprocal temperature, and a least-squares fit to the data yields an activation energy of $E_{th}^*=4.9$ meV close to the spectroscopic displacement of the unresolved doublet line (Ga1)* from $(Ga1)^0$. Figure 4 also shows the temperature dependence of $(Ga1)^0$. We ascribe the drop of the $(Ga1)^0$ intensity above 20 K exclusively to thermal dissociation of the luminescent defect state disregarding temperature effects due to vibronic coupling which was shown to be weak. The data in Fig. 4 are fitted by an expression

$$I(T)/I(0)=[1+C_1\exp(-E_1/kT) + T^{3/2}C_2\exp(-E_2/kT)]^{-1}$$

describing the activation of charge carriers localized in the luminescent $(Ga1)^0$ state into a band (activation energy E_2, factor $T^{3/2}$ due to band density of states) via an intermediate bound state (activation energy E_1). The parameter set obtained from a least-squares fit to the data is

$$E_1=E_{th}^*=4.9 \text{ meV (given)}, \quad C_1=0.2 ,$$

$$E_2=12.3 \text{ meV} \quad C_2=11.8 \text{ K}^{-3/2} .$$

The thermal dissociation energy 12.3 meV of the luminescent Ga1 state is much lower than the spectroscopic displacement of the Ga1 line from the band edge which reflects the total electron-hole binding energy and amounts to $E_{spectr}=1.1695-0.8754$ eV$=294.1$ meV. Figure 4 shows the level scheme as derived from the thermal data. We conclude that the optical defect represents a strong

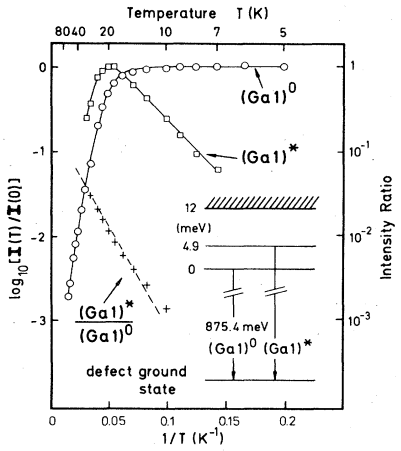

FIG. 4. Temperature dependence of the no-phonon $(Ga1)^0$ transition and of the unresolved lines $(Ga1)_1^0$ and $(Ga1)_2^0$ jointly labeled (Ga1)*. A least-squares fit to the intensity ratios of $(Ga1)^0$ and (Ga1)* yields 4.9-meV activation energy consistent with the spectroscopic spacings [5.1 and 6.0 meV of $(Ga1)_1^0$ or $(Ga1)_2^0$, respectively, from $(Ga1)^0$]. The inset shows the level scheme as deduced from the thermal data.

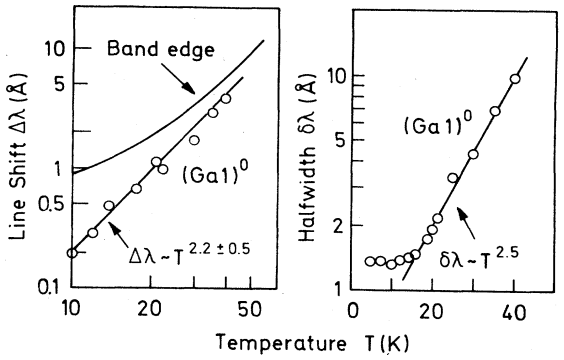

FIG. 5. $(Ga1)^0$ line shift and half-width as a function of temperature.

binding potential for a particle which is primarily bound and that a second particle is then weakly localized with an energy corresponding to the thermal dissociation energy of ≈ 12 meV. This model is confirmed by the Zeeman data which suggest a tightly bound hole. The defect can therefore be viewed as a pseudodonor. The low-lying excited states, $(Ga1)_1^0$ and $(Ga1)_2^0$, could then be valley-orbit states of the electron. Unfortunately, photoluminescence-excitation (PLE) spectroscopy able to confirm the pseudodonor model by the detection of effective-mass-like excited electron states and successfully applied to other defect spectra in silicon[11,12] could not be employed in the present system, owing to the disadvantageous wavelength range of the Ga1 spectrum.

To complete the temperature-dependent data we have measured the half-width and the shift of the $(Ga1)^0$ line as a function of temperature (Fig. 5). The half-width is $\delta\lambda\approx 1.3$ Å up to 15 K and then increases as $T^{2.5}$. The wavelength of $(Ga1)^0$ shifts following a $T^{2.2}$ law for $10<T<40$ K different from the band-edge shift which is depicted in Fig. 5 for comparison using literature data.[13] The significant discrepancy between the shift of the band edge and the $(Ga1)^0$ line is consistent with the Ga1 center being a deep defect.

III. ISOTOPE EFFECTS

Usually, the Ga1 spectrum was generated by electron irradiation and appropriate annealing of silicon doped with gallium in the bulk. In a few cases high-purity floating-zone silicon was implanted with ^{69}Ga or ^{71}Ga isotopes. In the implanted samples, identical spectra were observed; in particular, there was no detectable shift of the $(Ga1)^1$ local-mode satellite within 0.1% of the vibration quantum energy. On a harmonic oscillator model, a gallium isotope effect would be expected to be of order of $1-\sqrt{69/71}\,\hat{=}\,1.4\%$. Therefore, we conclude that Ga does not play a role in the 56.3-meV vibration mode. Moreover, we have not observed a Ga isotope shift in the NP transition. The vibration energy of 56.3 meV is rather close to the 58.1 meV of the momentum conserving TO phonon (as derived from shallow bound exciton spectra) or to the peak in the TO-phonon density of states of the

lattice. Therefore, the present mode may be a slightly modified TO lattice-phonon coupling to the electronic transition in which no isotope effects are expected. In this context we recall that the O^{Γ} phonon gives rise to a distinct satellite of the $(Ga1)^0$ line (Fig. 2). To our knowledge, no literature data exist on infrared absorption of irradiated Ga-doped silicon which could be compared to the present 56.3-meV vibration mode.

A positive isotope effect was found after the ^{69}Ga implantation of a crystal which was ^{13}C enriched in the bulk to a relative concentration of $[^{13}C]:[^{12}C]=1.3:1$ (Fig. 6). The concentration ratio known from the starting material was confirmed by observing the intensities of the local modes (E and E') of the damage-induced G line (0.97 eV) (Refs. 2–4); their carbon isotope effect is essentially due to the vibration of one carbon atom per optical center.[4] The $(Ga1)^0$ line shows a large carbon isotope splitting of 0.12 meV with an intensity ratio of the two components of 65:35. The isotope splitting demonstrates that the optical defect incorporates carbon. However, with the relative isotope concentrations given, the ratio is inconsistent with any number of carbon atoms per optical center. Assuming equal optical activity for ^{12}C and ^{13}C, the intensity of the various possible isotopic combinations in a defect incorporating n carbon atoms can be described by a polynomial $(a+b)^n$, with a and b being the relative isotope concentrations. Therefore, one always expects more intense isotopic components on the side of the ^{13}C unit in Fig. 6, irrespective of the exact spectral positions of the mixed isotopic combinations between the "pure" combinations made up from ^{12}C or ^{13}C alone.

This leads to our conclusion that the experimental intensities in Fig. 6 are not relevant, and that the ^{13}C-enriched sample may have been contaminated with ^{12}C during the Ga implantation process. This can occur with a diffusion pump at a poor vacuum; however, our vacuum was better than 10^{-6} Torr or $\approx 10^{-4}$ Pa. (Other implantation data were energy of ion beam 350 keV, dose $\approx 10^{16}$ cm^{-2}, and temperature $T \lesssim 50$ °C.) As the penetration depth of the exciting laser light is only a few micrometers, the luminescence signals are sensitive to the conditions of a thin surface layer and additional ^{12}C if contamination on the silicon surface could influence the signals. After repeated anneals at 100–150 °C, the relative intensities of the two peaks in the upper spectrum of Fig. 6 changed towards an $\sim 1:1$ intensity ratio supporting our suspicion that the original relative intensities are due to an artifact.

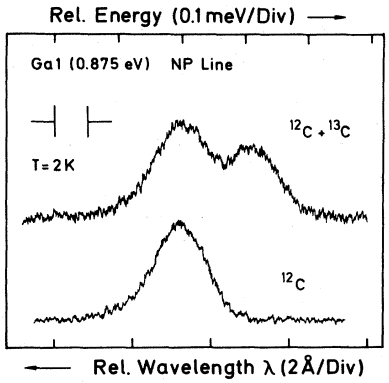

FIG. 6. Carbon isotope effect in the $(Ga1)^0$ no-phonon line. Lower trace: spectrum in sample containing carbon in natural abundances. Upper trace: spectrum in ^{13}C-enriched sample to concentrations $[^{12}C]:[^{13}C]=1:1.3$.

A deconvolution of the double-peak spectrum in the ^{13}C-enriched sample (upper trace, Fig. 6) suggests that the spectrum is made up of only two components with the lower energy peak at the exact position of the ^{12}C peak in the nonenriched sample (lower trace in Fig. 6). The latter result was obtained at low laser excitation with the sample immersed in pumped helium after numerous measurements had shown that at higher excitation powers the ^{12}C peaks in the two spectra are slightly shifted against each other due to the temperature dependence of the Ga1 line position [cf. also Fig. 5(a)]. This result corrects our recent conclusion (based on a slight shift between the two ^{12}C peaks) that at least two carbon atoms are involved.[9] We note that ^{13}C has no influence on the local-mode satellites.

IV. UNIAXIAL-STRESS MEASUREMENTS

Uniaxial stress up to 500 MPa was applied along ⟨001⟩, ⟨111⟩, and ⟨110⟩ axes of crystals cut as parallelepipeds (typical sizes $2\times2\times8$ mm^3) and with the long axis parallel to the stress. The experiments were performed in a temperature-controlled Dewar so that also the splitting of the excited state lines $(Ga1)^0_1$ and $(Ga1)^0_2$ could be observed.

In Fig. 7, we compare the splitting patterns of the $(Ga1)^0$ line and the $(Ga1)^1$ local-mode satellite at medium-stress values. For each stress direction, the same number of stress-induced components and almost equal relative intensities are observed in either transition. Apart from other arguments presented above we consider this direct proof of $(Ga1)^1$ being a quasilocalized-mode satellite of $(Ga1)^0$.

The stress response of $(Ga1)^0$ is shown in detail in Fig. 8. The line splits into two, two, and three components when the stress is directed along ⟨001⟩, ⟨111⟩, or ⟨110⟩, respectively. The stress response is nonlinear in all cases due to mixing with $(Ga1)^0_1$ and $(Ga)^0_2$ states.

Spectra showing the splitting of all three no-phonon lines at selected stress values are shown in Fig. 9. We

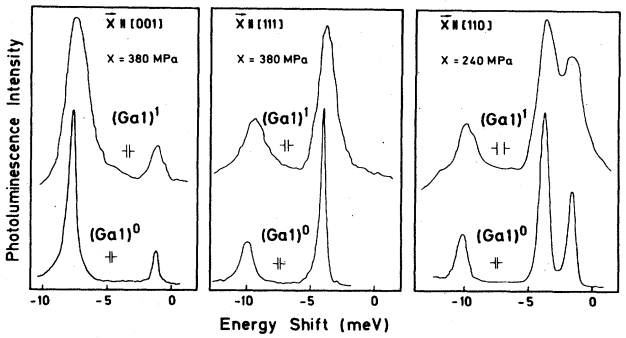

FIG. 7. Comparison of uniaxial stress splitting of $(Ga1)^0$ no-phonon line and $(Ga1)^1$ local-mode satellite at selected stress values.

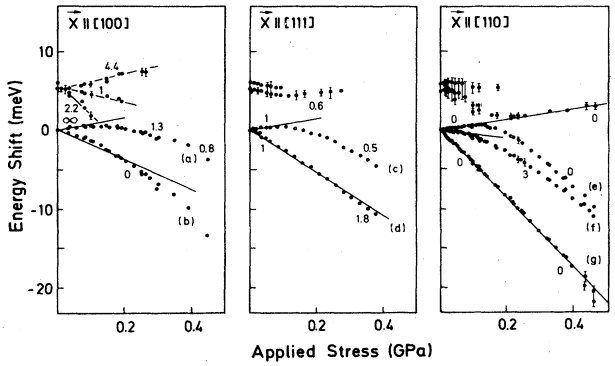

FIG. 8. Uniaxial stress splitting of the three no-phonon transitions $(Ga1)^0_0$, $(Ga1)^0_1$, and $(Ga1)^0_2$. Energy scale normalized to $(Ga1)^0_0$ zero-stress position. Solid lines for $(Ga1)^0_0$ components correspond to fit using the piezo-optical constants A_1, A_2, and A_3 given in the text. Numbers at the curves denote the degree of polarization expressed as the intensity ratio of π- to σ-polarized contributions in a component. Solid lines for $(Ga1)^0_1$ and $(Ga1)^0_2$ are only guides for the eye. Line labels (a) through (g) are independent of the defect orientations a through f in Figs. 14 and 15.

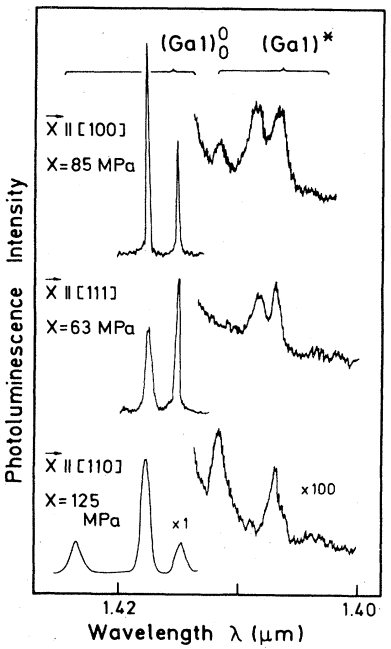

FIG. 9. Selected spectra of the no-phonon transitions [$(Ga1)^0_0$, $(Ga1)^0_1$, and $(Ga1)^0_2$] under uniaxial stress (the latter lines are here jointly labeled Ga1*).

were not able to resolve and to distinguish components developing from the closely spaced $(Ga1)^0_1$ or $(Ga1)^0_2$ lines for each stress direction. This situation is expressed by using once more the common label (Ga1)* in Fig. 9. We find three components for $\mathbf{X}||[100]$, two components for $\mathbf{X}||[111]$, and up to three resolved components for $\mathbf{X}||[110]$.

The splitting of (Gal)* is also nonlinear and the mixing of the three electronic upper states is evident from the asymptotic stress behavior: For $\mathbf{X}||[110]$, e.g., the high-energy component of $(Ga1)^0$ interacts with the low-energy component of (Ga1)* and both lines exchange their linear splitting rate exhibited at low- or high-stress values far away from the interaction regime. In addition, there is an intensity increase of the weak (Ga1)* branch by a factor of 30 when it approaches the $(Ga1)^0$ branch also reflecting the admixture of the strong $(Ga1)^0$ component. At higher-stress values, the (Ga1)* branch loses intensity rapidly possibly due to thermalization into lower-energy states.

We have not made attempts to fit the $(Ga1)^0$ stress response quantitatively in a perturbation approach taking into account the mixing with $(Ga1)^0_1$ and $(Ga1)^0_2$ states: nine splitting and nine interaction parameters would be necessary in the secular matrix unfavorable for an unambiguous fit. However, we determine the symmetry of the defect from the linear splitting in the low-stress regime. When low stress is directed along any of the three crystal axes (as in Fig. 8) and the temperature is varied from 4.2 to ≈ 10 K we do not observe thermalization between the stress-induced components. Therefore we conclude that all splittings are due to the lifting of orientational degeneracy and that electronic degeneracies do not play a role. Under this assumption, the observed numbers of components for the individual stress orientations are characteristic of rhombic I (C_{2v}) symmetry; using standard theoretical results,[14] we find the set of piezo-optical constants (in units of meV/GPa) fitting the linear-stress response:

$$A_1 = 8.0, \quad A_2 = -18.6, \quad \text{and } A_3 = \pm 25.4 .$$

For further discussion we note that the corresponding eigenvalues of the piezospectroscopic tensor A_{ij} (same units) are

$$\lambda_1 = A_1 = 8.0, \quad \lambda_2 = A_2 + A_3 = 6.8 ,$$

and

$$\lambda_3 = A_2 - A_3 = -44 .$$

Clifton *et al.*[10] in their stress study on the Ga1 line also derived C_{2v} symmetry of the defect and obtained a similar parameter set:

$$A_1 = 8.3, \quad A_2 = -14.5, \quad \text{and } A_3 = \pm 20.4 .$$

In rhombic I symmetry, the $(Ga1)^0$ line corresponds to a π oscillator along the z axis of the defect (such an oscillator is labeled "σ oscillator" in the table of Ref. 14).

There is a denoted polarization change of the stress-induced components when the stress is increased (Fig. 8). Referring to a specific case like $\mathbf{X}||[100]$, the change represents a difficulty in understanding the data: Component (a) is emitted by a center which is compressed by the stress along its C_2 rotation axis, and this particular perturbation is described by the stress component σ_{zz}. In C_{2v}, σ_{zz} can mix exclusively states belonging to the same representation (e.g., Γ_1 is mixed by σ_{zz} only with Γ_1; see

Appendix A), and hence polarization changes are impossible. A solution of this problem comes from Zeeman experiments (see Sec. V), where it is shown that the upper and lower states of the $(Ga1)^0$ line transform as Γ_5 with the inclusion of the spin. The polarization of transitions between such states of noninteger momenta is not uniquely determined as the products of representations $\Gamma_5 \otimes \Gamma_5$ appearing in the perturbation matrix elements contain all irreducible representations $\Gamma_1+\Gamma_2+\Gamma_3+\Gamma_4$ (see Appendix A). If one of the excited upper defect states preferentially emits σ-polarized radiation we can explain the stress data: Two states transforming as Γ_5 are mixed by the σ_{zz} stress component, thus giving rise to nonlinear splittings and a related change of polarization. In all other respects, the Γ_5 states behave like states $\Gamma_1,\Gamma_2,\Gamma_3,\Gamma_4$ (Appendix A) and, therefore, lead to the same *linear* stress splitting.

The temperature dependence of the stress-induced components was studied at various stress values and for stress along the crystal axes $\langle 001 \rangle$ and $\langle 111 \rangle$. An example for $\mathbf{X} \| \langle 111 \rangle$ is shown in Fig. 10, where we plot the intensities of the two components c and d and their intensity ratio. At a stress value where c and d are spectroscopically split by $\Delta E_{\text{spectr}} = 5.6$ meV, the thermal activation energies of the components are ≈ 12 meV (c) and ≈ 8 meV (d), the energy difference of the upper transition states therefore being ≈ 4 meV. The intensity ratio of c and d follows an exponential law from 20 K and higher with an activation energy of $\Delta E_{\text{th}} \approx 5$ meV consistent with the former value of ≈ 4 meV. As transition c has 5.6 meV larger photon energy than d, the lower states must be inversely ordered with an energy separation of ≈ 10 meV. The level scheme is depicted in Fig. 10. The situation described here has reproducibly been found for stress along $\langle 001 \rangle$ and $\langle 111 \rangle$, and independent of the stress value this situation obeys an approximate relationship $\Delta E_{\text{th}} \approx -\Delta E_{\text{spectr}}$ entailing analogous level schemes as in Fig. 10.

Such temperature-dependent intensity ratios of the stress-induced components must be related with the reorientation of the defect under stress since two components observed at different spectral positions are emitted by centers occupying nonequivalent orientations in the lattice. The defect reorients at temperatures as low as 20 K, indicating that the reorientation is essentially electronic in nature requiring no substantial displacement of defect atoms from their sites. Moreover, the ease of the process hints to interstitial defect constituents as being chiefly responsible for atomic motions necessary for the reorientation. Our data also suggest that there is a threshold for the reorientation roughly proportional to the applied stress: The drop of the intensity ratio of the stress-induced components starts at a temperature which is low for low stress and high for high stress. We note that the reorientation is not due to a Jahn-Teller effect needing an electronic degeneracy which is absent in C_{2v} symmetry. However, as has been discussed in the literature, off-center distortions can occur without the need of an electronic degeneracy.[15,16]

For completeness, we describe the results of a further stress experiment which remains not understood. When at constant temperature (≈ 5 K) the stress is varied the induced line components show opposite behavior for the various stress directions (Fig. 11). The ratio of b/a for $\mathbf{X} \| [100]$ increases, the ratio of d/c for $\mathbf{X} \| [111]$ decreases, and both ratios are expressible by an exponential law

$$\exp(\alpha \Delta E_{\text{th}}/kT)$$

where $|\alpha| < 0.1$. The ratios for $\mathbf{X} \| [110]$ show no simple functional dependence. These effects in the $(Ga1)^0$ spectrum are unclear and principally difficult to separate from the mixing-in of the $(Ga1)^*$-line components by the stress.

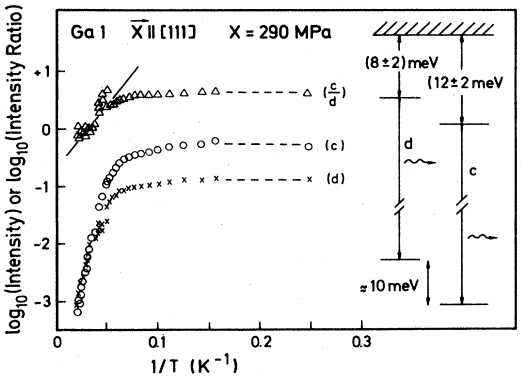

FIG. 10. Temperature dependence of stress-induced components c and d exhibited for $\mathbf{X} \| [111]$ and their intensity ratio, c/d. The stress corresponds to a spectroscopic splitting of 5.6 meV between c and d. The slope (solid line) corresponds to $\approx$4-meV thermal activation energy. Activation energies at $T \gtrsim 20$ K for c and d are 12±2 meV or 8±2 meV, respectively. The level scheme combines thermal and spectroscopic data.

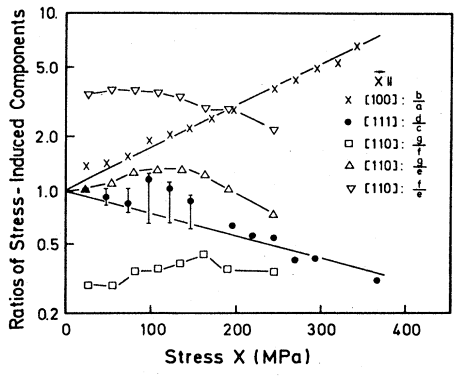

FIG. 11. Intensity ratios of stress-induced components at ≈ 5 K as a function of stress. Ratios for $\mathbf{X} \| [100]$ and $\mathbf{X} \| [111]$ tend to "thermalization" or "antithermalization" of the components, respectively, both with thermal energies below 10% of the spectroscopic spacing of the components involved.

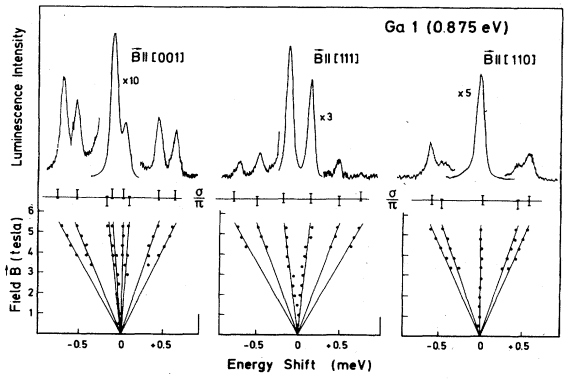

FIG. 12. Zeeman splitting of $(Ga1)^0$ no-phonon line and Zeeman spectra at 5.3 T. Energies normalized to zero-field position of line. σ/π scales indicate polarization of the components. Light observation perpendicular to field **B** (Voigt configuration).

V. ZEEMAN MEASUREMENTS

Zeeman measurements were performed up to fields of $B=5.3$ T in Voigt configuration (observation perpendicular to **B**) or Faraday configuration (observation parallel to **B**). For **B** along [001], [111], and [110] in perpendicular observation, the $(Ga1)^0$ line splits linearly with the applied field strength B and shows anisotropic behavior (Fig. 12). As the most striking feature, there are for each direction, intense inner components stronger by a factor of ≈ 10 than the outer components. For **B**||[001], we observe two π- and two σ-polarized inner components which can only be distinguished using polarizers in the measurement. All four outer components are σ polarized. For **B**||[111], there are two strong inner unpolarized components, and two low- and two high-energy outer components which are σ or π polarized, respectively. For **B**||[110], the single strong inner component is unpolarized, and one component of the two weak line pairs observed on its high- and low-energy sides is π polarized. In parallel observation and **B**||[110] (Fig. 13), two extra-strong inner components appear, and all three components are totally polarized. For **B**||[100] in parallel observation, only two inner components remain, and all components are unpolarized including the outer ones.

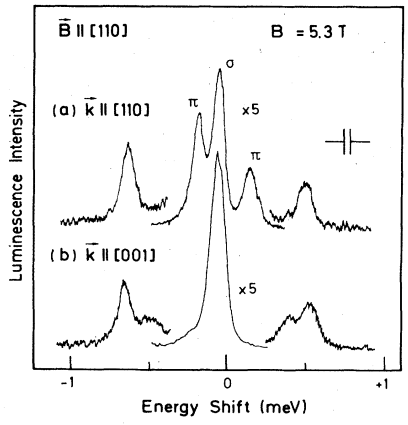

FIG. 13. Zeeman spectra for **B**||[110] in (a) parallel and (b) perpendicular observation.

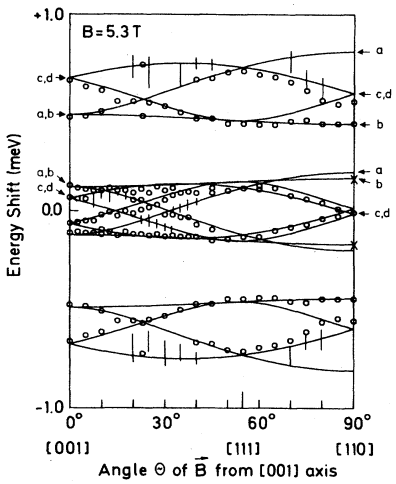

FIG. 14. Angular dependence of Zeeman spectra when the magnetic field is rotated from [001] to [110] in the $(1\bar{1}0)$ plane. Vertical bars denote broad components. Solid lines represent fit for a Γ_5 to Γ_5 transition in rhombic I (C_{2v}) symmetry. For g values, see text. The origin of some of the Zeeman components from different defect orientations is indicated (cf. Fig. 15).

The angular dependence of the $(Ga1)^0$ Zeeman spectrum in Voigt configuration is shown in Fig. 14, where a magnetic field of 5.3 T is rotated in the $(1\bar{1}0)$ plane from [001] to [110]. Additional components arise for angles $0°<\theta<50°$, but the pattern simplifies for $\theta\approx 55°$ (i.e., **B**||[111]) when several inner components fall together and only two components remain observable up to an angle of 90°. In contrast, two components at symmetric positions with respect to the unshifted line at zero field appear for $\theta=90°$ in Faraday configuration in Fig. 14 as was already mentioned above (see Fig. 13). Quantitatively, the splitting of the outer components from the zero of energy correspond to a g value of about 2.

The total set of Zeeman data can be understood in a model where the $(Ga1)^0$ transition is due to a $s=\frac{1}{2}$ to $s=\frac{1}{2}$ transition (i.e., $\Gamma_5\rightarrow\Gamma_5$) in rhombic I (C_{2v}) symmetry. Basically, a transition between two states of spin $\frac{1}{2}$ is intuitive, as it explains the strength of the inner components ($\Delta S_z=0$) which need no spin flip, and the weakness of the outer components which are related with a spin flip ($\Delta s_z=\pm 1$) and become weakly allowed by a (small) spin-orbit coupling. The inner components correspond to a π oscillator along the z axis of the defect, consistent with the result of the stress measurements. The outer components correspond to elliptic σ oscillators: The spin is quantized along the defect axis and not along the magnetic field direction.

In the C_{2v} model, the inner components of the centers a and b (Fig. 15) are unobservable in Faraday configuration for **B**||[001] and in Voigt configuration for **B**||[110] consistent with the experiments (Figs. 13 and 14) when simple dipole-emission characteristics of the oscillators are as-

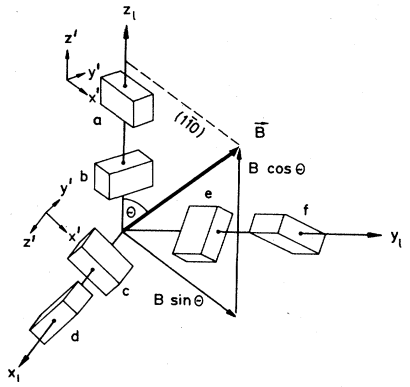

FIG. 15. Illustration of possible orientations a through f of a rhombic I (C_{2v}) symmetric defect. [The labels are independent of the notation (a) through (g) used in Fig. 8 to characterize the stress-split components of the $(Ga1)_0^0$ line.] Defect coordinates x',y',z', laboratory coordinates x_l,y_l,z_l.

sumed. It is striking that the anisotropy of the outer components is very similar to the anisotropy of the inner components. This suggests that one of the states between which the transition occurs splits isotropically in the magnetic field, whereas the anisotropy is totally due to the other states. On this assumption the splitting between the outer and inner components corresponds to $g_{iso}=2$. The anisotropic state is described in rhombic I symmetry by three values g_x, g_y, and g_z (Appendix B). The fit in Fig. 14 (solid lines) uses the set of parameters

$$g_x=3.3,\quad g_y=0.9,\quad \text{and } g_z=1.2\ ,$$

where g_x and g_y principally cannot be distinguished and are exchangeable. The effective g value is $g_{eff}=\frac{1}{3}(g_x+g_y+g_z)=1.8$. Details of the spectra in Fig. 13 show that the σ oscillator corresponding to the $(\frac{1}{2}\rightarrow-\frac{1}{2})$ transition is not circular but elliptic as expected in rhombic I symmetry. In Faraday configuration, $\mathbf{k}||\mathbf{B}||[110]$, the two components of the weak outer-line pairs, which are closest to the strong central components disappear. They stem from the b defect in Fig. 15 and become unobservable in this observation mode when intensity $y \gg$ intensity x of the elliptic oscillator is assumed; the same assumption also explains the π polarization of the outer b components for $\mathbf{B}||[110]$ in Voigt configuration [Fig. 13(a)]. The ratios of g_x, g_y, and g_z are similar to the corresponding ratios of the eigenvalues of the piezospectroscopic tensor

$$g_x:g_y:g_z \approx \lambda_3:\lambda_2:\lambda_1\ .$$

We cannot decide whether this rough coincidence of the ratios is accidental or physically significant. If it is physical, the anisotropic response to stress or magnetic fields could be related to the geometrical structure of the defect, and the large differences of g_x,g_y and λ_2,λ_3 could then indicate that the defect has essentially planar structure, i.e., the atoms of the defect are all positioned in one plane.

On the basis of the data thus far presented, the Ga1 line can be attributed to the radiative recombination of an electron with a hole at the defect. The pair is not strongly coupled as the Zeeman data can only be understood in terms of an $S=\frac{1}{2}$ to $S=\frac{1}{2}$ transition. Similarly, the spectroscopic binding energy ($E_{spectr}=294.1$ meV) is much larger than the thermal dissociation energy ($E_{th}=12$ meV) indicating that only one particle is tightly bound. Consistency with the Zeeman data is obtained when this particle is assumed to be the hole. The rhombic potential quenches the orbital momentum of the hole (or splits the orbital hole states into $m_l=0$ and $m_l=\pm1$ with $m_l=0$ being the lowest) by an energy large compared to the Zeeman energy and produces the strongly anisotropic hole-"spin" state. A small remaining portion of the orbital momentum may be responsible for the value $g_{eff}=1.8<2$ of this state and may cause the weak outer Zeeman components to appear, which are related with a spin flip. The electron is then loosely bound with an extended wave function and behaves like a quasifree particle of isotropic spin $\frac{1}{2}$. The opposite model of a tightly bound electron and a loosely bound hole is discarded: A tightly bound electron would be expected to have isotropic $g=2$, but a hole as weakly localized as revealed by ≈12 meV thermal activation energy should virtually exhibit the fourfold Zeeman splitting of a Γ_8 particle in T_d.

The relative strength of the outer Zeeman components in Figs. 12 and 13 are comparable, indicating that there is no thermal population of the respective transition initial states. By contrast, thermalization between the inner components is obviously accomplished to a higher degree, the whole situation being best illustrated in the upper spectrum of Fig. 13. When the excitation power is varied by a factor of 10, the central components show little effect whereas the outer components change much more in intensity. Although these effects are entirely unclear, they could be related with long spin-lattice relaxation times particularly for the loosely bound electron as is, e.g., well documented in the case of phosphorus bound electrons in silicon,[17,18] and amount to values τ_{sl} as large as half an hour at low temperatures.

VI. DISCUSSION

Up to now several Ga-related centers in silicon have been reported in the literature. Most intensely studied is the substitutional Ga acceptor.[19] At low temperatures the neutral Ga acceptor can bind an exciton, and Ga bound exciton spectra have also been investigated in some detail, both in emission[20] and absorption.[21] Recently it was shown that all acceptors in silicon except for Tl possess associated "acceptor X" centers; X was identified as carbon, and the centers were identified as acceptor-carbon pairs occupying nearest-neighbor substitutional lattice sites.[22] Usually, the GaX center is a grown-in defect like the other acceptor-X centers, but Rome *et al.*[23] reported that the defect can also be created by neutron irradiation of Ga-doped float-zone silicon. A different center is the Ga-related defect responsible for the EPR G22 spectrum which is created by electron irradiation of Ga-doped silicon and was identified as a trigonal Ga pair

$(Ga_s^- + Ga_i^{2+})$ on substitutional and nearest-neighbor interstitial lattice sites.[24,25]

The luminescent defects Ga1, Ga2, and Ga3 are different from the species above as the structural properties derived from the PL measurements are not consistent with any of these defects. In the following, we summarize those results from the preceding sections which are essential in a discussion of the microscopic defect model: (1) The defect has rhombic I (C_{2v}) symmetry, i.e., it possesses two reflection planes perpendicular to each other and a twofold rotation axis in the line of intersection of the planes. (2) The defect incorporates Ga and C atoms. It is possible that more than one Ga atom is involved, and almost conclusive that a single C atom is involved. (3) The thermal data show that under stress along ⟨100⟩ and ⟨111⟩, the defect reorients when the temperature is raised above $\approx$20 K. This feature suggests that the reorientation is of electronic nature, i.e., temperature causes a rearrangement of electronic bonds related with only small atomic displacements of (possibly interstitial) defect constituents whereas no essential atomic reorientations occur. (4) The form of the piezospectroscopic tensor and the g tensor of the deeply bound hole indicate that the center is particularly sensitive to fields applied along its x' axis (defect coordinate system) which could most easily be understood by assuming a virtually "planar" defect configuration.

The simplest model meeting these requirements would consist of a gallium-carbon pair directed along a ⟨001⟩ axis and sharing a substitutional lattice site. When this defect unit is compact, i.e., when the gallium and carbon atoms are sufficiently close together compared to the four neighbor silicon atoms it could easily reorient between different ⟨001⟩ directions. The defect has a C_{2v} point-group symmetry, but when the electron and the hole wave functions are more concentrated on one of the defect atoms than on the other, as plausible from the different valences of Ga and C in the model, the partial configuration (Si—C—Si plus Ga) or (Si—Ga—Si plus C), respectively, in {110} planes could acquire preferential importance and determine the behavior of the excited defect state under uniaxial stress and magnetic fields. This gallium-carbon pair model has recently also been mentioned by Clifton *et al.* in conjunction with their uniaxial stress measurements as a possible model, however, on a much narrower experimental basis than presented in this work (as an example, the incorporation of carbon in the defect was speculatively anticipated).

In several cases [e.g., in the above-mentioned G line or the I_2 line (1.080 eV) (Ref. 26)] isotope effects occurring in the local-mode satellites of the no-phonon transition were helpful in identifying atomic defect constituents. The Ga1 spectrum shows neither a Ga nor a C isotope effect in the 56.3 meV local-mode line. In addition a Si isotope effect [as in a local-mode satellite of the C line (0.79) spectrum[7,9]] is not detectable. Therefore, none of these atoms plays a vital role in the local vibration. On the other hand, the quantum energy of 56.3 meV is relatively close to the TO(X) phonon frequency of the lattice and it seems plausible that the vibration is essentially a TO lattice mode slightly perturbed by the presence of the optical defect.

In summary, we have studied the Ga1 photoluminescence spectrum as a function of isochronal anneal time in temperature-controlled emission experiments and in uniaxial stress and magnetic fields. A carbon isotope effect observed in the no-phonon transition was discussed as giving evidence of a single carbon atom being optically active in the defect. The results are sufficient to rule out many defect models but they are not strong enough for an unambiguous deduction of a defect model. A specific possible model was discussed. Further progress seems to be mainly confined to the study of the carbon isotope effect, and such work is in progress.

ACKNOWLEDGMENTS

It is a pleasure to thank G. D. Watkins (Lehigh University, Bethlehem, Pennsylvania) for supplying ^{13}C-enriched silicon samples and for many helpful discussions, and W. Letzel and G. Pensl (Institut für Angewandte Physik, Universität Erlangen, Federal Republic of Germany) for ^{69}Ga and ^{71}Ga isotope implantations. Thanks are due to L. Raschke and G. Steudle (Institut für Strahlenphysik, Universität Stuttgart) for the irradiation of silicon crystals. We are grateful to Ms. U. Schall (Physikalisches Institut, Teil 4, Universität Stuttgart) for repeated measurements of the carbon isotope effect and A. Dörnen (Physikalisches Institut, Teil 4, Universität Stuttgart) for enlightening discussions on group-theoretical aspects in the interpretation of the stress and Zeeman data. R. C. Newman (University of Reading, United Kingdom) helpfully supported our search for literature on Ga-related infrared absorption measurements. We are also obliged to G. Davies and collaborators (Physics Department, King's College, University of London, United Kingdom) for privately communicating their data (Ref. 10) prior to publication. The financial support of the Deutsche Forschungsgemeinschaft (Contract No. Sa-311/2) is gratefully acknowledged.

APPENDIX A

The most general secular matrix in first-order perturbation is derived, which describes the shift and the interaction of states under uniaxial stress transforming as the one-dimensional representations Γ_1, Γ_2, Γ_3, and Γ_4 of the rhombic I (C_{2v}) point group. Bases of these representations in the defect coordinates are[27]

$$\Gamma_1:\ (x')^2,(y')^2,(z')^2\ ,$$

$$\Gamma_2:\ x'z'\ ,$$

$$\Gamma_3:\ x'y'\ ,$$

$$\Gamma_4:\ y'z'\ .$$

The laboratory coordinates are chosen to be

$$x=(1/\sqrt{2})(x'+y')\ ,$$

$$y=(1/\sqrt{2})(-x'+y')\ ,$$

$$z=z'$$

(i.e., a rotation by $\pi/4$ about the z axis).

The perturbation potential describing the energy shifts of the states due to the stress is given by the dyadic product of an electronic operator $\vec{\vec{\gamma}}$ and the stress $\vec{\vec{\sigma}}$

$$V=\sum_{i,j}\gamma_{ij}\sigma_{ij} ,$$

where the σ_{ij} transform as the products x_ix_j $(x_i,x_j=x,y,z)$ and are related with the external stress $\mathbf{X}$ as

$$\sigma_{ij}=|\mathbf{X}|\cos(\mathbf{X},\mathbf{i})\cos(\mathbf{X},\mathbf{j})$$

with $\mathbf{i},\mathbf{j}$ unit vectors along x,y,z. The energy shift ΔE is given by the matrix elements of V and does not depend on the coordinate system. Therefore, it transforms as Γ_1 and the sum in V contains only products of such γ and σ elements which transform according to the same irreducible representation in C_{2v}. The form of V is thus derived to be

$$V=\gamma_1\sigma_{zz}+\gamma_1'(\sigma_{xx}+\sigma_{yy})+\gamma_1''\sigma_{xy}+\gamma_2(\sigma_{xz}+\sigma_{yz})$$
$$+\gamma_3(\sigma_{yy}-\sigma_{xx})+\gamma_4(-\sigma_{xz}+\sigma_{yz}) .$$

Here the subscripts of the electronic operators γ_r denote the representations contributing to the respective terms.

We define matrix elements of the γ_r with the states transforming as $\Gamma_1,\ldots,\Gamma_4$:

$$\langle\Gamma_1/\gamma_1/\Gamma_1\rangle=A_1 ,$$
$$\langle\Gamma_1/\gamma_1'/\Gamma_1\rangle=A_2 ,$$
$$\langle\Gamma_1/\gamma_1''/\Gamma_1\rangle=2A_3 ,$$

and

$$\langle\Gamma_i/\gamma_2/\Gamma_j\rangle=D_{ij} ,$$
$$\langle\Gamma_i/\gamma_3/\Gamma_j\rangle=E_{ij} ,$$
$$\langle\Gamma_i/\gamma_4/\Gamma_j\rangle=F_{ij} .$$

(More precisely, these matrix elements should be written as differences of two matrix elements in the upper and lower transition states each of which has the form given above: in the experiments we measure only differences of level shifts.)

The total interaction matrix is symmetric and is written as

	Γ_1	Γ_2	Γ_3	Γ_4
Γ_1	$A_1\sigma_{zz}+A_2(\sigma_{xx}+\sigma_{yy})+2A_3\sigma_{xy}$	$D_{12}(\sigma_{xz}+\sigma_{yz})$	$E_{13}(\sigma_{yy}-\sigma_{xx})$	$F_{14}(\sigma_{yz}-\sigma_{xz})$
Γ_2	$D_{12}(\sigma_{xz}+\sigma_{yz})$	$A_1'\sigma_{zz}+A_2'(\sigma_{xx}+\sigma_{yy})+2A_3'\sigma_{xy}$	$F_{23}(\sigma_{yz}-\sigma_{xz})$	$E_{24}(\sigma_{yy}-\sigma_{xx})$
Γ_3	$E_{13}(\sigma_{yy}-\sigma_{xx})$	$F_{23}(\sigma_{yz}-\sigma_{xz})$	$A_1''\sigma_{zz}+A_2''(\sigma_{xx}+\sigma_{yy})+2A_3''\sigma_{xy}$	$D_{34}(\sigma_{xz}+\sigma_{yz})$
Γ_4	$F_{14}(\sigma_{yz}-\sigma_{xz})$	$E_{24}(\sigma_{yy}-\sigma_{xx})$	$D_{34}(\sigma_{xz}+\sigma_{yz})$	$A_1'''\sigma_{zz}+A_2'''(\sigma_{xx}+\sigma_{yy})+2A_3'''\sigma_{xy}$

The diagonal elements are those which are contained in the table given by Kaplyanskii.[14] Our notation for the corresponding piezo-optical constants A_1, A_2, and A_3 confirm with Kaplyanskii's notation. States with half-integral total angular momentum are split by a C_{2v} crystal field into substates transforming as Γ_5 (the only additional representation in the double group in C_{2v}). The effect of stress on Γ_5 is described by the matrix element $\langle\Gamma_5/V/\Gamma_5\rangle$, which yields in detail

	Γ_5^-	Γ_5^+
Γ_5^-	$A_1\sigma_{zz}+A_2(\sigma_{xx}+\sigma_{yy})+2A_3\sigma_{xy}+iE(\sigma_{xz}+\sigma_{yz})$	$D(\sigma_{xx}-\sigma_{yy})+iF(\sigma_{xz}-\sigma_{yz})$
Γ_5^+	$-D(\sigma_{xx}-\sigma_{yy})+iF(\sigma_{xz}-\sigma_{yz})$	$A_1\sigma_{zz}+A_2(\sigma_{xx}+\sigma_{yy})+2A_3\sigma_{xy}-iE(\sigma_{xz}+\sigma_{yz})$

Because Kramers degeneracy cannot be lifted by stress the constants D, E, and F must vanish. Therefore, only real diagonal elements are left and these are the same as for Γ_1, Γ_2, Γ_3, Γ_4 states. The product $\Gamma_5\otimes\Gamma_5=\Gamma_1+\Gamma_2+\Gamma_3+\Gamma_4$ contains contributions from all one-dimensional representations, so that three π oscillators can be emitted which have different intensities and are quantized along x', y', and z' in the defect system.

APPENDIX B

The most general Zeeman Hamiltonian

$$\mathcal{H}_{\text{Zee}}=\mu_B\mathbf{S}\cdot\vec{\vec{g}}\cdot\mathbf{B}$$

of a $s=\frac{1}{2}(\Gamma_5)$ state in C_{2v} point-group symmetry is derived. $\mathscr{H}_{\text{Zee}}$ transforms as Γ_1. In the T_d point group, **B** transforms as Γ_4, therefore the product $\mu_B \mathbf{S}\cdot\overleftrightarrow{g}$ also transforms as Γ_4. In C_{2v}, $\Gamma_5(T_d)$ splits as $\Gamma_5\rightarrow\Gamma_2+\Gamma_3+\Gamma_4$, and the Zeeman matrix contains three terms:

$$\langle\Gamma_5/\mathscr{H}_{\text{Zee}}/\Gamma_5\rangle = c_1 B_y\langle\Gamma_5/\Gamma_2/\Gamma_5\rangle + c_2 B_z\langle\Gamma_5/\Gamma_3/\Gamma_5\rangle + c_3 B_x\langle\Gamma_5/\Gamma_4/\Gamma_5\rangle .$$

The total magnetic interaction matrix can be written as

$$\begin{array}{c} \\ \Gamma^5_{-1/2} \\ \Gamma^5_{+1/2} \end{array} \begin{array}{c} \begin{array}{cc} \Gamma^5_{-1/2} & \Gamma^5_{+1/2} \end{array} \\ \begin{bmatrix} g_z B_z & g_x B_x + i g_y B_y \\ g_x B x - i g_y B_y & -g_z B_z \end{bmatrix} \end{array} .$$

This is the same matrix which is obtained when in the Zeeman Hamiltonian

$$\mathscr{H}_{\text{Zee}} = \mu_B \mathbf{S}\cdot\overleftrightarrow{g}\cdot\mathbf{B}$$

one takes the spin-$\frac{1}{2}$ matrices for **S** and

$$\overleftrightarrow{g} = \begin{bmatrix} g_x & 0 & 0 \\ 0 & g_y & 0 \\ 0 & 0 & g_z \end{bmatrix}$$

for the $\overleftrightarrow{g}$ tensor.

[1] J. R. Noonan, C. G. Kirkpartrick, and B. G. Streetman, Solid State Commun. **15**, 1055 (1974).

[2] K. Thonke, H. Klemisch, J. Weber, and R. Sauer, Phys. Rev. B **24**, 5874 (1981), and previous references therein.

[3] K. D. O'Donnell, K. M. Lee, and G. D. Watkins, Physica **116B**, 258 (1983).

[4] G. Davies, E. C. Lightowlers, and M. doCarmo, J. Phys. C **16**, 5503 (1983), and further references therein.

[5] J. Wagner, K. Thonke, and R. Sauer, Phys. Rev. B **29**, 7051 (1984), and previous references therein.

[6] K. Thonke, G. D. Watkins, and R. Sauer, Solid State Commun. **51**, 127 (1984).

[7] G. Davies, E. C. Lightowlers, R. Woolley, R. C. Newman, and A. S. Oates, J. Phys. C **17**, L499 (1984).

[8] K. R. Elliott, Phys. Rev. B **25**, 1460 (1982).

[9] K. Thonke, N. Bürger, G. D. Watkins, and R. Sauer, in Proceedings of the 13th International Conference on Defects in Semiconductors, Coronado, CA, 1984, edited by L. C. Kimmerling and J. M. Parsey, Jr. [J. Electron. Mater. **14a**, 823 (1985)].

[10] P. Clifton, G. Davies, and E. C. Lightowlers, J. Phys. C **17**, L889 (1984).

[11] J. Wagner and R. Sauer, Phys. Rev. B **26**, 3502 (1982).

[12] J. Wagner, A. Dörnen, and R. Sauer, Phys. Rev. B **31**, 5561 (1985).

[13] W. Bludau, A. Onton, and W. Heinke, J. Appl. Phys. **45**, 1846 (1974).

[14] A. A. Kaplyanskii, Opt. Spectrosc. **16**, 329 (1964).

[15] F. Bridges, CRC Crit. Rev. Solid State Sci. **5**, 1 (1975).

[16] M. D. Glinchuk, in *Modern Problems in Condensed Matter Sciences,* edited by Yu E. Perlin and M. Wagner (North-Holland, Amsterdam, 1984), Vol. 7, p. 819.

[17] G. Feher and E. A. Gere, Phys. Rev. **114**, 1245 (1959).

[18] H. Nagashima and H. Yamazaki, J. Phys. Soc. Jpn. **41**, 711 (1976).

[19] D. W. Fischer and J. J. Rome, Phys. Rev. B **27**, 4826 (1983), and previous references therein.

[20] M. A. Vouk and E. C. Lightowlers, J. Lumin. **15**, 357 (1977), and further references therein.

[21] K. R. Elliott, G. C. Osbourn, D. L. Smith, and T. C. McGill, Phys. Rev. B **17**, 1808 (1978), and further references therein.

[22] C. E. Jones, D. Schafer, W. Scott, and R. J. Hager, J. Appl. Phys. **52**, 5148 (1981).

[23] J. J. Rome, W. C. Mitchel, G. J. Brown, D. W. Fischer, M. C. Ohmer, and T. L. Peterson, Appl. Phys. Lett. **41**, 254 (1982).

[24] G. D. Watkins, in *Radiation Effects in Semiconductors,* edited by P. Baruch (Dunod, Paris, 1984), p. 97.

[25] G. D. Watkins, IEEE Trans. Nucl. Sci. **NS-16**, 13 (1969).

[26] K. Thonke, J. Weber, J. Wagner, and R. Sauer, Physica **116B**, 252 (1983).

[27] G. F. Koster, J. O. Dimmock, R. G. Wheeler, and H. Statz, *Properties of the Thirty-Two Point Groups* (MIT Press, Cambridge, 1963).